

The Impact of a Variable Mixing Efficiency on the Abyssal Overturning

CASIMIR DE LAVERGNE

Sorbonne Universités (UPMC, Univ. Paris 06)-CNRS-IRD-MNHN, LOCEAN Laboratory, Paris, France

GURVAN MADEC

Sorbonne Universités (UPMC, Univ. Paris 06)-CNRS-IRD-MNHN, LOCEAN Laboratory, Paris, France, and National Oceanography Centre, Southampton, United Kingdom

JULIEN LE SOMMER

CNRS-Université Grenoble Alpes, Laboratoire de Glaciologie et Géophysique de l'Environnement, Grenoble, France

A. J. GEORGE NURSER

National Oceanography Centre, Southampton, United Kingdom

ALBERTO C. NAVEIRA GARABATO

University of Southampton, National Oceanography Centre, Southampton, United Kingdom

(Manuscript received 19 December 2014, in final form 22 May 2015)

ABSTRACT

In studies of ocean mixing, it is generally assumed that small-scale turbulent overturns lose 15%–20% of their energy in eroding the background stratification. Accumulating evidence that this energy fraction, or mixing efficiency R_f , significantly varies depending on flow properties challenges this assumption, however. Here, the authors examine the implications of a varying mixing efficiency for ocean energetics and deep-water mass transformation. Combining current parameterizations of internal wave-driven mixing with a recent model expressing R_f as a function of a turbulence intensity parameter $Re_b = \varepsilon_\nu / \nu N^2$, the ratio of dissipation ε_ν to stratification N^2 and molecular viscosity ν , it is shown that accounting for reduced mixing efficiencies in regions of weak stratification or energetic turbulence (high Re_b) strongly limits the ability of breaking internal waves to supply oceanic potential energy and drive abyssal upwelling. Moving from a fixed $R_f = 1/6$ to a variable efficiency $R_f(Re_b)$ causes Antarctic Bottom Water upwelling induced by locally dissipating internal tides and lee waves to fall from 9 to 4 Sverdrups (Sv; 1 Sv $\equiv 10^6 \text{ m}^3 \text{ s}^{-1}$) and the corresponding potential energy source to plunge from 97 to 44 GW. When adding the contribution of remotely dissipating internal tides under idealized distributions of energy dissipation, the total rate of Antarctic Bottom Water upwelling is reduced by about a factor of 2, reaching 5–15 Sv, compared to 10–33 Sv for a fixed efficiency. The results suggest that distributed mixing, overflow-related boundary processes, and geothermal heating are more effective in consuming abyssal waters than topographically enhanced mixing by breaking internal waves. These calculations also point to the importance of accurately constraining $R_f(Re_b)$ and including the effect in ocean models.

1. Introduction

Away from its boundaries, where heat and freshwater exchanges with the atmosphere, cryosphere, and solid earth form and destroy water masses, buoyancy forcing

of the ocean occurs almost exclusively via mixing. Though mixing along density surfaces was shown to drive significant net densification and attendant downwelling through the cabbeling and thermobaric effects (Iudicone et al. 2008a; Klocker and McDougall 2010), mixing across isopycnals is thought to be responsible for most of the interior water mass transformation (Munk and Wunsch 1998). A key process controlling the diabatic component of the meridional overturning

Corresponding author address: Casimir de Lavergne, LOCEAN Laboratory, 4 Place Jussieu, F-75005 Paris, France.
E-mail: casimir.delavergne@gmail.com

circulation, diapycnal mixing thus exerts a major influence on the global distribution of temperature, salinity, and biogeochemical tracers. Observed ocean properties and transport budgets at the basin scale suggest diapycnal eddy diffusivities averaging about $10^{-4} \text{ m}^2 \text{ s}^{-1}$ below 1000-m depth (Munk 1966; Munk and Wunsch 1998; Ganachaud and Wunsch 2000; Lumpkin and Speer 2007; Talley 2013). Yet this value masks strongly inhomogeneous mixing rates, with background values about one order of magnitude lower and localized enhanced rates up to two orders of magnitude higher (Toole et al. 1994; Munk and Wunsch 1998; Wunsch and Ferrari 2004; Waterhouse et al. 2014).

The strong spatial and temporal heterogeneity of turbulent mixing constitutes a challenge both for the representativeness of direct measurements of mixing rates and for its realistic representation in ocean models. Though ad hoc prescription of vertical diffusivities has long prevailed in numerical ocean modeling (e.g., Bryan and Lewis 1979), progress has been achieved with the development of energetically constrained parameterizations that compute diffusivities from specified dissipation rates of internal wave energy (Huang 1999; St. Laurent et al. 2002; Polzin 2009; Olbers and Eden 2013). However, in converting dissipation rates into a diapycnal diffusivity, such parameterizations rely on the knowledge of the mixing efficiency: that is, the fraction of the energy of breaking waves that actually serves to irreversibly mix the fluid.

It is commonly assumed that about one-sixth of the energy flux into turbulence contributes to diapycnal mixing, the remainder being lost as heat via viscous friction. Cross-validated estimates of diapycnal diffusivity from open ocean observations often support mixing efficiencies of 15%–25% (Toole et al. 1994; Ledwell et al. 1998, 2000), although an overall broader range of about 0%–40% has been reported (e.g., Ruddick et al. 1997; St. Laurent and Schmitt 1999). In contrast, basin-scale inferences (Stigebrandt 1976; de Young and Pond 1989; Stigebrandt and Aure 1989; Arneborg and Liljebladh 2001) and in situ observations at strongly mixing sites (Inall 2009; Bouffard and Boegman 2013; Bluteau et al. 2013) have consistently shown lower efficiencies to prevail. Recently, drawing on a large body of numerical and laboratory results, as well as field measurements, a turbulent diffusivity model that accounts for observed variability in mixing efficiency has been designed for studies of stratified turbulence (Shih et al. 2005; Bouffard and Boegman 2013). Here, we combine this new model with current parameterizations of mixing induced by breaking internal waves to investigate the implications of a varying mixing efficiency for ocean energetics and deep-water mass transformation. A description of the variable

efficiency model follows (section 2). In section 3, we apply the variable R_f model to mixing driven by breaking internal tides and lee waves and revise former estimates of water mass transformation by internal wave-driven mixing (de Lavergne et al. 2015, manuscript submitted to *J. Phys. Oceanogr.*, hereinafter LMSNG). We discuss implications for the maintenance of the abyssal overturning circulation in section 4 and provide conclusions in section 5.

2. The turbulent diffusivity model

Current parameterizations of ocean mixing (St. Laurent et al. 2002; Polzin 2009; Olbers and Eden 2013) assume that the turbulent kinetic energy produced by the breaking of internal waves (ε_T) contributes in fixed proportions to a downward buoyancy flux ($K_\rho N^2$) and frictional heat production (ε_ν):

$$\varepsilon_T = \varepsilon_\nu + K_\rho N^2, \quad (1)$$

with

$$K_\rho N^2 = R_f \varepsilon_T, \quad \varepsilon_\nu = (1 - R_f) \varepsilon_T, \quad (2)$$

where K_ρ is the eddy diffusivity of density, N^2 is the buoyancy frequency, and R_f is the mixing efficiency, usually taken to be one-sixth. The latter choice means that turbulent overturns lose about 17% of their energy in raising dense water parcels over lighter ones, thus eroding the local stratification and fluxing buoyancy downward. Although frictional heating consumes most of the turbulent kinetic energy, it is generally ignored, for it represents a quasi-negligible buoyancy source in the ocean interior (LMSNG). This simple mixing model derives from the pioneering work of Osborn (1980), who argued that, given a steady-state balance between turbulent kinetic energy production, viscous dissipation, and vertical buoyancy exchange, the mixing sink term $K_\rho N^2$ should not exceed 15%–20% of the shear production ε_T . Because of difficulty in accurately estimating mixing efficiency from field measurements and for lack of deeper knowledge of its variability, this maximum value of the mixing efficiency has since served as a reference for field and modeling studies of shear-induced turbulent mixing.

However, it was soon recognized that the buoyancy flux should be proportionately less in weakly stratified waters (Osborn 1980). Indeed, in the limit of a homogeneous fluid, turbulent stirring cannot drive buoyancy exchange nor modify the potential energy of the system, and all of the turbulent kinetic energy must dissipate through friction. More generally, as the restoring gravity force becomes weak compared to stirring forces, turbulent

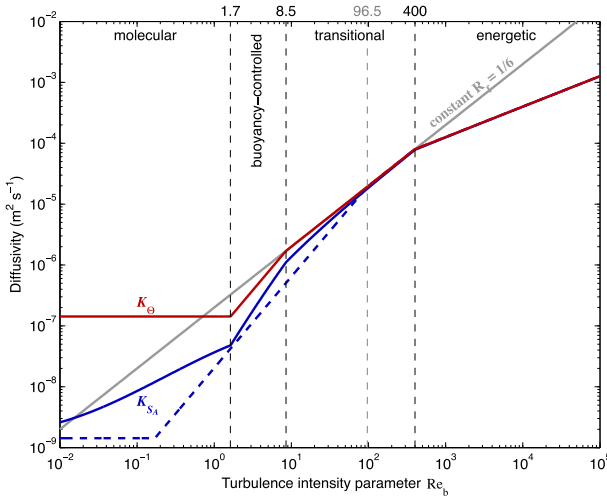


FIG. 1. Turbulent diffusivity model based on Bouffard and Boegman (2013) and Jackson and Rehmann (2014). Shown is the diapycnal diffusivity (m^2s^{-1}) of heat (red) and salt (blue) as a function of the turbulence intensity parameter. The dashed blue curve corresponds to the salt diffusivity parameterized by Bouffard and Boegman (2013), whereas the solid blue curve is deduced from the heat diffusivity (red), using the diffusivity ratio parameterization of Jackson and Rehmann (2014). Indicated regimes at the top only refer to the heat diffusivity. The thick gray line shows the Re_b dependence of diffusivities assuming a constant mixing efficiency of one-sixth. Solid red and blue curves will be referred to as the variable R_f model in subsequent calculations.

overturns become less susceptible to perform work against gravity and more susceptible to viscous damping. Thus, as stratification decreases to very low levels, it is required that R_f also approaches zero. Consistent with these theoretical expectations, the past two decades have seen a growing number of studies, based on direct numerical simulations, laboratory experiments, or field work, documenting reduced mixing efficiencies in actively mixing or weakly stratified waters (Gloor et al. 2000; Barry et al. 2001; Jackson and Rehmann 2003; Rehmann and Koseff 2004; Shih et al. 2005; Inall 2009; Davis and Monismith 2011; Hult et al. 2011; Dunckley et al. 2012; Bouffard and Boegman 2013; Bluteau et al. 2013).

In attempts to synthesize the vast spectrum of available data, several such studies have proposed that eddy diffusivities can be expressed as a function of a turbulence intensity parameter, $\text{Re}_b = \varepsilon_\nu / \nu N^2$, with ν the molecular kinematic viscosity of seawater, according to different Re_b regimes (Barry et al. 2001; Shih et al. 2005; Bouffard and Boegman 2013). Here, we adopt the most recent, field-validated parameterization of Bouffard and Boegman (2013), with a refinement offered by the parameterization of differential diffusion by Jackson and Rehmann (2014) (Fig. 1). The turbulence intensity parameter may be seen as the ratio of the destabilizing

force of turbulence to the stabilizing forces of stratification and viscosity (Barry et al. 2001). Since the oceanic range of molecular viscosity is roughly $1\text{--}2 \times 10^{-6} \text{m}^2\text{s}^{-1}$, with almost uniform values in the deep ocean, Re_b essentially measures the competing roles of turbulent stirring and stratification damping. At high Re_b , inertial forces overwhelm buoyancy forces, and turbulence becomes largely unaffected by stratification.

The Re_b dependence of heat and salt diffusivities proposed by Bouffard and Boegman (2013) is plotted in Fig. 1 (red and dashed blue). For $\text{Re}_b \geq 96.5$, both diffusivities are equal, and $K_\rho = K_\Theta = K_{S_A}$, where Θ denotes conservative temperature and S_A denotes absolute salinity. Within the range $96.5 \leq \text{Re}_b \leq 400$,

$$K_\rho = 0.2\nu \text{Re}_b, \tag{3}$$

which is equivalent to (2) with $R_f = 1/6$. Hence, the typical mixing efficiency of one-sixth is valid only for these moderate Re_b values (transitional regime), corresponding to $K_\rho = 1.9\text{--}8 \times 10^{-5} \text{m}^2\text{s}^{-1}$. In the higher Re_b range (energetic regime), mixing efficiency is reduced compared to the high-end value:

$$K_\rho = 4\nu\sqrt{\text{Re}_b}, \quad R_f = 1/(1 + 0.25\sqrt{\text{Re}_b}). \tag{4}$$

According to (4), increasingly strong turbulence intensities (as measured by Re_b) lead to increasingly small mixing efficiencies. In other words, as turbulence grows uninhibited by stratification, the energy input to small-scale turbulence becomes increasingly inefficient at driving a buoyancy flux, consistent with physical arguments. In particular, the buoyancy flux vanishes together with the stratification:

$$K_\rho N^2 = 4\sqrt{\nu\varepsilon_\nu}N \xrightarrow{N \rightarrow 0} 0, \tag{5}$$

thus satisfying the necessary property mentioned above. We also note that the predicted $K_\rho = 4\sqrt{\varepsilon_\nu\nu}N^{-1}$ in the energetic regime is analogous to the dependence of K_ρ on stratification suggested by the field data compilation of Gargett (1984), assuming a constant $\varepsilon_\nu \sim 10^{-9} \text{W kg}^{-1}$.

At lower Re_b , turbulent mixing becomes increasingly controlled by buoyancy effects. Incomplete mixing can then favor upgradient fluxes, implying reduced mixing efficiencies relative to the transitional regime (Holt et al. 1992; Merryfield 2005; Bouffard and Boegman 2013). Because molecular diffusion of salt is two orders of magnitude slower than that of heat, reversible mixing of salt can occur at larger turbulence intensities, explaining the narrower validity of the transitional regime for K_{S_A} than for K_Θ . We use a recently proposed Re_b -dependent

parameterization of the diffusivity ratio K_{S_A}/K_Θ (Jackson and Rehmann 2014; see appendix) to deduce an alternative form of K_{S_A} from K_Θ (Fig. 1, solid blue). Both parameterizations show reasonable qualitative agreement, with weak differential diffusion for $Re_b \geq 50$ and increasingly small diffusivity ratio toward the molecular regimes. In the following, we use the form of K_{S_A} deduced from the Jackson and Rehmann (2014) diffusivity ratio, as it offers a well-constrained, slightly improved parameterization of differential diffusion. Nevertheless, we find that differential diffusion and the reduced R_f in the buoyancy-controlled regime have almost negligible impact on large-scale water mass transformation by breaking internal waves. This follows from the fact that most of the wave-breaking energy falls within the transitional and energetic regimes: the bulk of buoyancy fluxes is driven by relatively energetic turbulence, with $Re_b \sim O(10^2-10^5)$. Therefore, the discussion will henceforth be focused on the role of reduced mixing efficiencies in high-diffusivity regions.

3. Application to internal wave-driven mixing

a. Methods

The saturation of diapycnal mixing for low stratification or high mixing energy has strong implications for ocean energetics and the abyssal ocean circulation. Indeed, wave breaking and mixing occur primarily along topographically complex ocean boundaries (e.g., Waterhouse et al. 2014), in localized mixing hot spots, so most of the turbulent activity takes place where mixing efficiency is expected to be reduced. To quantify the impact of variable efficiencies on the overturning circulation, we apply the Re_b -dependent mixing model to constructed climatologies of stratification and internal wave energy dissipation.

Significantly, underlying the application to gridded mean fields of dissipation and stratification is the assumption that the $K_\rho(Re_b)$ model is robust to a leap in scale from localized, time-varying turbulence to large-scale, time-mean environmental conditions. Developed from laboratory-scale experiments and direct numerical simulations as well as field microstructure measurements, the Bouffard and Boegman (2013) parameterization was primarily designed for field studies inferring diffusivities from instantaneous profile measurements of the viscous dissipation of turbulent kinetic energy. Because of the nonlinearity of $K_\rho(Re_b)$ in the energetic regime, the direct applicability of the model to annual, large-scale means of N^2 and ε_ν may thus be questioned. In particular, wave-breaking events are known to be both localized and episodic so that transient

Re_b levels within turbulent patches may substantially exceed larger-scale, annual average turbulence intensities. Consequently, cumulative, large-scale mixing efficiencies reflecting the net irreversible mixing achieved by an ensemble of breaking events could be lower than efficiencies inferred from a global climatology of Re_b :

$$\overline{R_f(Re_b)^{\Delta x, \Delta y, t}} < R_f(\overline{Re_b}^{\Delta x, \Delta y, t}), \quad (6)$$

where the overbar denotes averaging over the resolved scales of the climatology. This suggests that our methodology is likely to underestimate the effect of reduced mixing efficiencies at high Re_b . On the other hand, local density gradients, including the deep stratification, could be underestimated in some places by a coarsely resolved hydrographic climatology, possibly biasing high the computed turbulence intensities. Clearly, further research is required to assess the scale dependence of mixing efficiency (see, e.g., Arneborg 2002; Ivey et al. 2008) and to finely calibrate the Re_b -dependent model for large-scale modeling applications. Nevertheless, the fact that the Bouffard and Boegman (2013) parameterization applied to multiple microstructure profiles yields diffusivities in broad agreement with larger-scale mixing rates inferred from tracer release experiments (e.g., Watson and Ledwell 2000) suggests that its use in a global climatological setting is not unreasonable. Moreover, the physical grounds that underpin the general behavior of the parameterized $R_f(Re_b)$ also hold at larger spatial and temporal scales. Thus, application of the turbulent diffusivity model described in section 2 to global climatologies of stratification and wave-breaking energy should yield a sensible first estimate of the sensitivity of deep internal wave-driven mixing to the assumed Re_b dependence of R_f .

Using published estimates of barotropic-to-baroclinic tidal conversion (Nycander 2005; Melet et al. 2013b) and lee-wave radiation (Scott et al. 2011), we first produce three-dimensional maps of locally dissipating internal tide and lee-wave energy (Figs. 2a,b). The power density distribution $\varepsilon_T(x, y, z)$ is determined by assuming that one-third of the wave energy dissipates where it is generated, spreading in the vertical according to an exponential decay from the seabed with a 500-m e -folding length (St. Laurent et al. 2002). The relatively well-constrained spatial structure of internal wave generation relative to wave dissipation motivates these partly arbitrary though widely used choices. Because we focus on sensitivity to mixing efficiency on a global scale, significant regional deviations of the inferred distribution of energy sinks from actual oceanic conditions should not undermine the present conclusions.

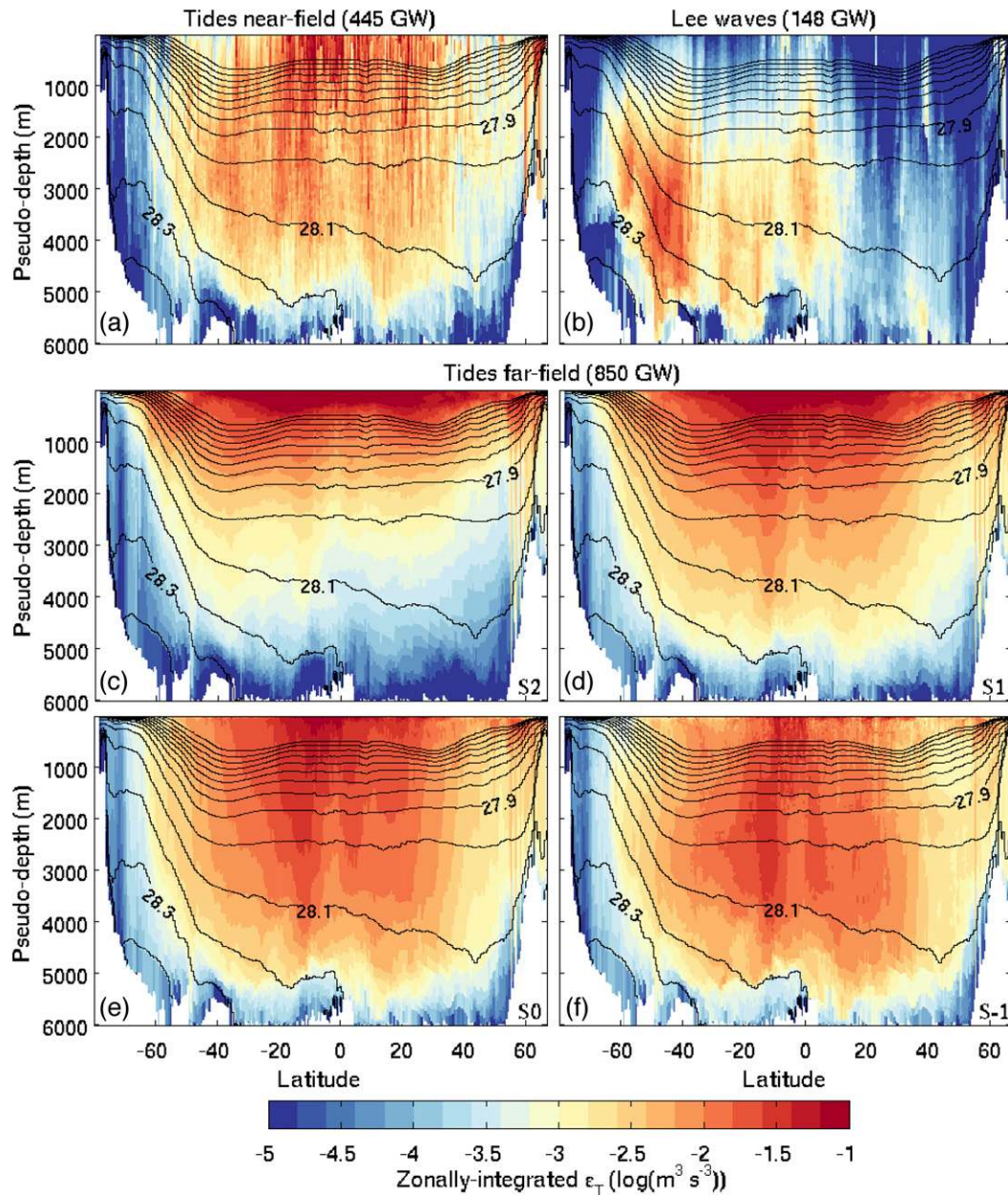


FIG. 2. Along-isopycnal zonal sum of wave-breaking energy ϵ_T [$\log(\text{m}^3 \text{s}^{-3})$] from locally dissipating (a) internal tides and (b) lee waves and from (c)–(f) remotely dissipating internal tides. The vertical structure of remote tidal dissipation is specified according to scenario (c) S2, (d) S1, (e) S0, or (f) S-1. Note that the density-binned values of zonally integrated ϵ_T are reprojected to pseudodepth for visual purposes. The remapping procedure involves a simple bottom-up filling of each latitude band with ocean grid cells ordered from dense to light. Neutral density surfaces within 27–28.5 kg m^{-3} are contoured every 0.1 kg m^{-3} .

Following LMSNG, we assume mixing to be suppressed for the remaining two-thirds of the lee-wave energy flux. This is justified by recent observational and modeling results revealing weaker dissipation rates than would be predicted from the presently used theoretical estimate (Sheen et al. 2013; Waterman et al. 2013, 2014; Nikurashin et al. 2014). However,

because the energy carried by low-mode internal tides that propagate away from generation sites could have an important role for the abyssal buoyancy budget (Oka and Niwa 2013; LMSNG), we construct idealized distributions of remote tidal dissipation as an attempt to explore the sensitivity of far-field tidal mixing to mixing efficiency (Figs. 2c–f). Guided by

published maps of column-integrated baroclinic tide dissipation (Niwa and Hibiya 2011), we specify the horizontal distribution of far-field dissipation by uniformly redistributing the remaining two-thirds of internal tide energy within a radius of 1000 km of generation sites. Admittedly, this procedure only grossly mimics the spreading of low-mode wave energy and oversimplifies a reality that should reflect specific pathways of the energy cascade, such as wave-wave interactions and topographic scattering (e.g., MacKinnon et al. 2013; Kelly et al. 2013; Eden and Olbers 2014). Nevertheless, earlier work showed that basin-scale water mass transformation is relatively insensitive to different plausible choices of the horizontal energy distribution over the open ocean (LMSNG). Much stronger sensitivity to the vertical distribution of far-field dissipation motivates the use of various scenarios for the vertical structure of wave-breaking energy (LMSNG): (S2) $\varepsilon_T \propto N^2$; (S1) $\varepsilon_T \propto N$; (S0) $\varepsilon_T \propto 1$; and (S-1) $\varepsilon_T \propto N^{-1}$. The numbering of the scenarios corresponds to exponents of N in the assumed dependence of dissipation to stratification. This choice of scenarios spans a fairly large range of possible structures (Figs. 2c-f), from pycnocline-intensified dissipation (S2 and S1) to preferential wave breaking in the abyss (S-1), thus providing probable bounds of transformation rates by far-field tidal mixing.

Next, we calculate the climatological buoyancy frequency from the World Ocean Circulation Experiment hydrographic atlas (Gouretski and Koltermann 2004), which provides annual mean fields at a resolution of $0.5^\circ \times 0.5^\circ$ in the horizontal and 10–250 m in the vertical. Computing diapycnal diffusivities and mixing efficiencies from the constructed N^2 and ε_T fields now only requires rewriting the Re_b -dependent model equations in terms of ε_T rather than ε_p (appendix). In the following, we use these constructed climatologies to contrast the traditional fixed R_f model (Fig. 1, gray) with the variable $R_f(\text{Re}_b)$ parameterization (Fig. 1, red and blue) for a range of metrics relevant to the large-scale circulation.

b. Buoyancy fluxes and potential energy

The diapycnal diffusivity and mixing efficiency associated with near-field mixing alone according to the fixed and variable efficiency models are depicted in Fig. 3. The density diffusivity is shown as a zonal mean ($\iint_\gamma K_\rho dS / \iint_\gamma dS$; Figs. 3a,b) or as a stratification-weighted zonal mean ($\iint_\gamma K_\rho N^2 dS / \iint_\gamma N^2 dS$; Figs. 3c,d) along surfaces of constant neutral density γ (Jackett and McDougall 1997). In contrast to the zonal average K_ρ , the stratification-weighted mean K_ρ is directly related to the buoyancy flux and will be referred to as an effective diffusivity. Effective diffusivities tend to be smaller than

mean diffusivities because of the correlation between strong mixing and weak stratification (Figs. 3a-d). Also conspicuous is the order of magnitude decrease in diffusivities over much of the ocean interior when moving from the constant to the variable R_f model. For instance, abyssal effective diffusivities do not exceed a few centimeters squared per second in the variable case, whereas $O(10) \text{ cm}^2 \text{ s}^{-1}$ values are common under a fixed efficiency. This implies that using the Re_b -dependent model causes a sharp, widespread reduction in mixing-induced buoyancy fluxes. Indeed, effective mixing efficiencies, calculated as $\iint_\gamma K_\rho N^2 dS / \iint_\gamma \varepsilon_T dS$, are strongly reduced in waters hosting significant energy dissipation (Figs. 2a,b, 3e,f), resulting in a global effective efficiency of only 7.3% for near-field mixing alone (Table 1).

The potential energy supplied by diapycnal mixing to the global ocean volume V may be calculated as follows:

$$\begin{aligned} \partial_t E_p &= g \iiint_V \partial_t \rho z dV \\ &= g \iiint_V [\partial_\Theta \rho \partial_z (K_\Theta \partial_z \Theta) + \partial_{S_A} \rho \partial_z (K_{S_A} \partial_z S_A)] z dV, \end{aligned} \quad (7)$$

where E_p denotes potential energy, ρ is the locally referenced potential density, and height z increases upward and has its origin at the surface. Concurrent with the reduction in mixing efficiency, the global potential energy supply by near-field mixing drops by 55% from fixed to variable R_f , resulting in a global input of only 44 GW (Table 1). This potential energy source is comparable to the ~ 35 GW supplied by geothermal heating (LMSNG), suggesting that geothermal heat fluxes are as important as bottom-intensified mixing by breaking internal waves to the maintenance of the abyssal stratification.

The constant R_f model also gives mixing efficiencies below one-sixth in a few places (Fig. 3e); this stems from the upper bound imposed on diapycnal diffusivities, chosen as $100 \text{ cm}^2 \text{ s}^{-1}$, required to avoid unrealistically large diffusivities at $\text{Re}_b > 5 \times 10^4$. This cap is also imposed on diffusivities predicted by the Bouffard and Boegman (2013) parameterization, but concerns many fewer grid cells, since such a high diffusivity is only reached at $\text{Re}_b = 6 \times 10^6$. Indeed, in contrast to the fixed R_f model, the variable R_f parameterization offers a smooth transition from the high-end mixing efficiency to fully saturated mixing, effectively pushing back the critical level at which additional energy can no longer increase buoyancy fluxes (Fig. 1).

The variable R_f model has a global mean mixing efficiency, $V^{-1} \iiint [(K_\rho N^2) / \varepsilon_T] dV$, that is much higher than the global effective efficiency, $\iiint K_\rho N^2 dV / \iiint \varepsilon_T dV$ (Table 1). Indeed, in the presence of near-field mixing

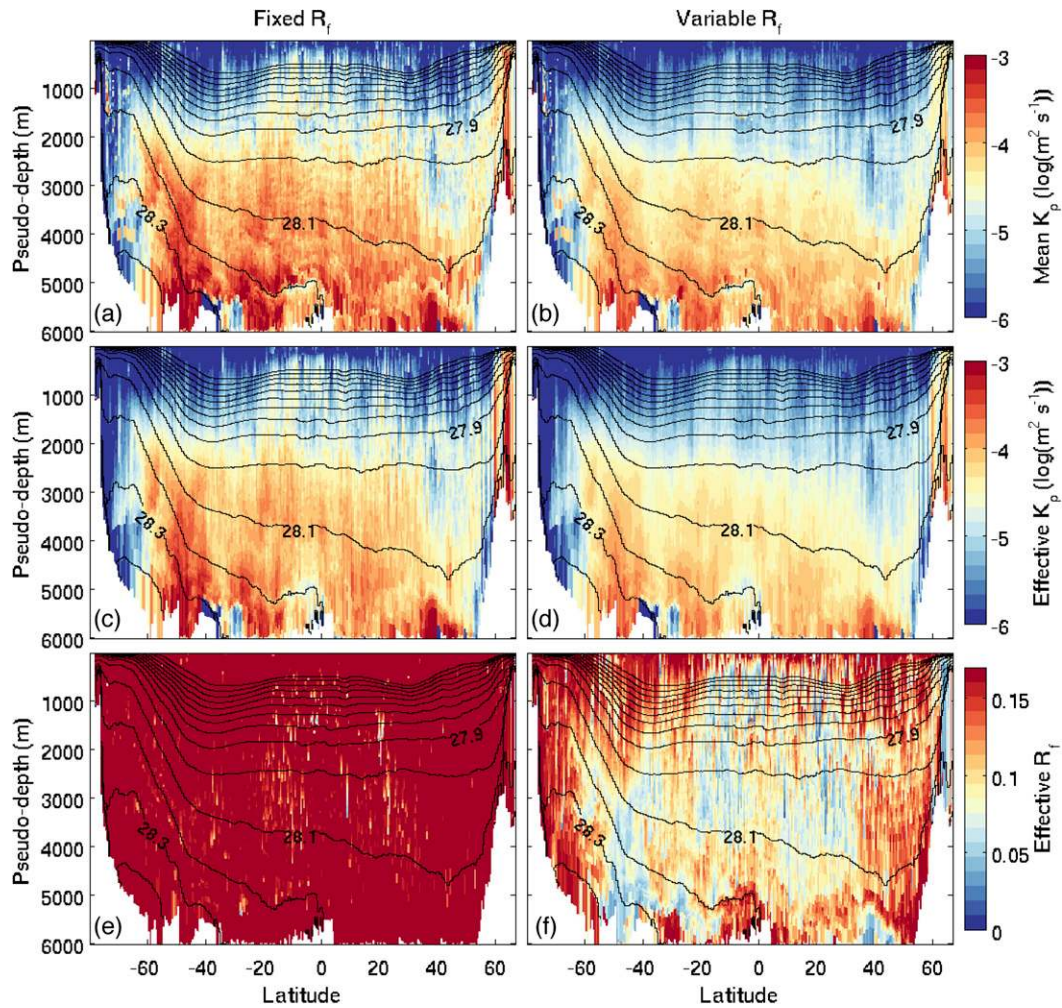


FIG. 3. Diffusivity [$\log(\text{m}^2 \text{s}^{-1})$] and mixing efficiency resulting from near-field mixing alone, according to (left) fixed and (right) variable efficiency models. Shown are along-isopycnal (a),(b) zonal mean diffusivity $\iint_{\gamma} K_p dS / \iint_{\gamma} dS$; (c),(d) stratification-weighted zonal mean diffusivity $\iint_{\gamma} K_p N^2 dS / \iint_{\gamma} N^2 dS$; and (e),(f) effective mixing efficiency $\iint_{\gamma} K_p N^2 dS / \iint_{\gamma} \epsilon_T dS$, where the density-binned values are projected to pseudodepth for visual purposes. Neutral density surfaces within 27–28.5 kg m^{-3} are contoured every 0.1 kg m^{-3} .

only, most of the ocean volume is characterized by moderate turbulence intensities belonging to the transitional regime, but those regions that fall within the energetic regime represent the bulk of internal wave

energy dissipation, implying a strong overall reduction in power contributing to mixing. The discrepancy is somewhat reduced when remote tidal dissipation is included (Table 1), as more energy dissipation occurs away

TABLE 1. Key characteristics of internal wave-driven mixing according to the fixed and variable mixing efficiency models. Values corresponding to the variable R_f parameterization are in parentheses.

	Global potential energy supply (GW)	Global effective R_f (%)	Global mean R_f (%)	AABW upwelling (30°S–67°N) (Sv)
Near-field only	97 (44)	15.8 (7.3)	16.6 (14.5)	9 (4)
Near- and far-field				
S2	161 (107)	16.3 (12.2)	16.6 (14.9)	10 (5)
S1	192 (129)	16.3 (11.7)	16.6 (14.9)	15 (8)
S0	224 (134)	16.1 (10.1)	16.6 (14.2)	25 (13)
S–1	231 (119)	15.6 (8.3)	16.5 (13.6)	33 (15)

from the weakly stratified near-bottom waters (Figs. 2, 4). Yet, even under the pycnocline-intensified wave breaking of scenarios S2 and S1, the addition of far-field energy dissipation does not always cause a commensurate increase in buoyancy fluxes, as would be expected from the assumption of a constant mixing efficiency.

Depending on the chosen scenario, the added contribution of remotely dissipating internal waves raises the global effective mixing efficiency to 8.3%–12.2% and the global potential energy supply to 107–134 GW (Table 1). The latter range can be compared to the 161–231 GW supplied by internal wave-driven mixing under a fixed efficiency and to the 240 GW that one would infer from the global energy input and assumptions of a constant $R_f = 1/6$ and a linear equation of state.¹ Though scenario S2 exhibits the largest effective mixing efficiencies, it has the lowest potential energy supply globally, a consequence of nonlinearity in the equation of state. Indeed, thermocline-intensified mixing causes significant net densification by transferring heat toward colder waters, which are less prone to thermal expansion. On the other hand, by enhancing dissipation away from the pycnocline, as assumed in scenario S–1, a similarly strong reduction in potential energy input results from saturating mixing in high Re_b waters. Thus, the combination of upper-ocean nonlinear effects and reduced efficiencies in the weakly stratified abyss appears to limit the overall potential energy source that may be derived from internal wave-driven mixing.

The lowest global effective efficiency is obtained for scenario S–1, which has the strongest energy dissipation in the deep ocean (Fig. 2), where the relatively weak stratification is unable to sustain proportionately strong buoyancy fluxes. Figure 4 illustrates the saturation of deep ocean mixing as more and more energy dissipation is placed at depth: whereas abyssal mixing levels markedly increase through scenarios S2 to S–1 under a fixed mixing efficiency (Figs. 4a,c,e,g), abyssal diffusivities show a much weaker enhancement when accounting for reduced mixing efficiencies at large Re_b (Figs. 4b,d,f,h). Hence, the impact of reduced mixing efficiencies is strongest in the abyssal ocean, with important implications for the consumption of Antarctic Bottom Water (AABW).

c. Water mass transformation

We calculate mixing-driven neutral density fluxes F_{eq}^γ and dianeutral transports T across neutral surfaces as follows (LMSG):

$$F_{\text{eq}}^\gamma = - \iiint_{\gamma \cong \gamma} [b \partial_\Theta \rho \partial_z (K_\Theta \partial_z \Theta) + b \partial_{S_A} \rho \partial_z (K_{S_A} \partial_z S_A)] dV \quad \text{and} \quad (8)$$

$$T = \partial_\gamma F_{\text{eq}}^\gamma, \quad (9)$$

where b is the ratio of the spatial gradients of neutral density and locally referenced potential density (Iudicone et al. 2008b). An equivalent diffusive flux of neutral density across a given neutral surface, resulting from temperature and salinity mixing below that surface is represented by F_{eq}^γ (de Lavergne et al. 2015).

Fluxes and transports associated with near-field mixing alone are shown in Fig. 5. North of 30°S, energy dissipation is dominated by internal tides (Fig. 2), and mixing drives a divergent neutral density flux over most of the interior density range, forcing net upward motion across neutral surfaces deeper than 27.2 kg m^{-3} (27.0 kg m^{-3}) under fixed (variable) R_f (Figs. 5a,b). The variable efficiency $R_f(Re_b)$ acts to moderate neutral density fluxes and dianeutral transports, reducing peak fluxes and transports by ~60%. In particular, the maximum rate of upwelling at the deep-/bottom water boundary ($\gamma = 28.11 \text{ kg m}^{-3}$) drops from 9 to 4 Sverdrups (Sv; $1 \text{ Sv} \equiv 10^6 \text{ m}^3 \text{ s}^{-1}$), implying that locally dissipating internal tides and lee waves may be unable to balance more than 4 Sv of northward bottom water flow out of the Southern Ocean.

In the Antarctic Circumpolar Current region, mixing is dominated by breaking lee waves (Fig. 2). Most energetic along the 28.15 kg m^{-3} neutral surface, lee waves drive a divergent density flux below that level and a convergent density flux above (Figs. 5c,d). Under the variable R_f model, buoyancy transfer from lighter ($\gamma \leq 28.15 \text{ kg m}^{-3}$) to denser ($\gamma \geq 28.15 \text{ kg m}^{-3}$) waters is damped, inducing both weaker upwelling of dense AABW and weaker downwelling of the overlying Circumpolar Deep Water. The net input to the bottom water layer south of 30°S is reduced from 2 Sv to less than 1 Sv. At lighter densities, the variable R_f formulation predicts even smaller transformation rates both north and south of 30°S, suggesting a weak overall influence of near-field mixing on the consumption of southward-flowing deep waters.

By accounting for the Re_b dependence of mixing efficiency, we show that focused near-bottom mixing as commonly parameterized for locally dissipating internal waves (St. Laurent et al. 2002) is only a minor contributor to the diabatic return of AABW. Nonetheless, if more widely distributed, as hypothesized in the present idealized scenarios, mixing driven by remotely breaking internal tides could be a more efficient driver of AABW

¹ Because of nonlinearities in the equation of state, the rate of change of potential energy given by (7) differs from $\iiint_V \rho K_\rho N^2 dV = \iiint_V \rho R_f \varepsilon_T dV$.

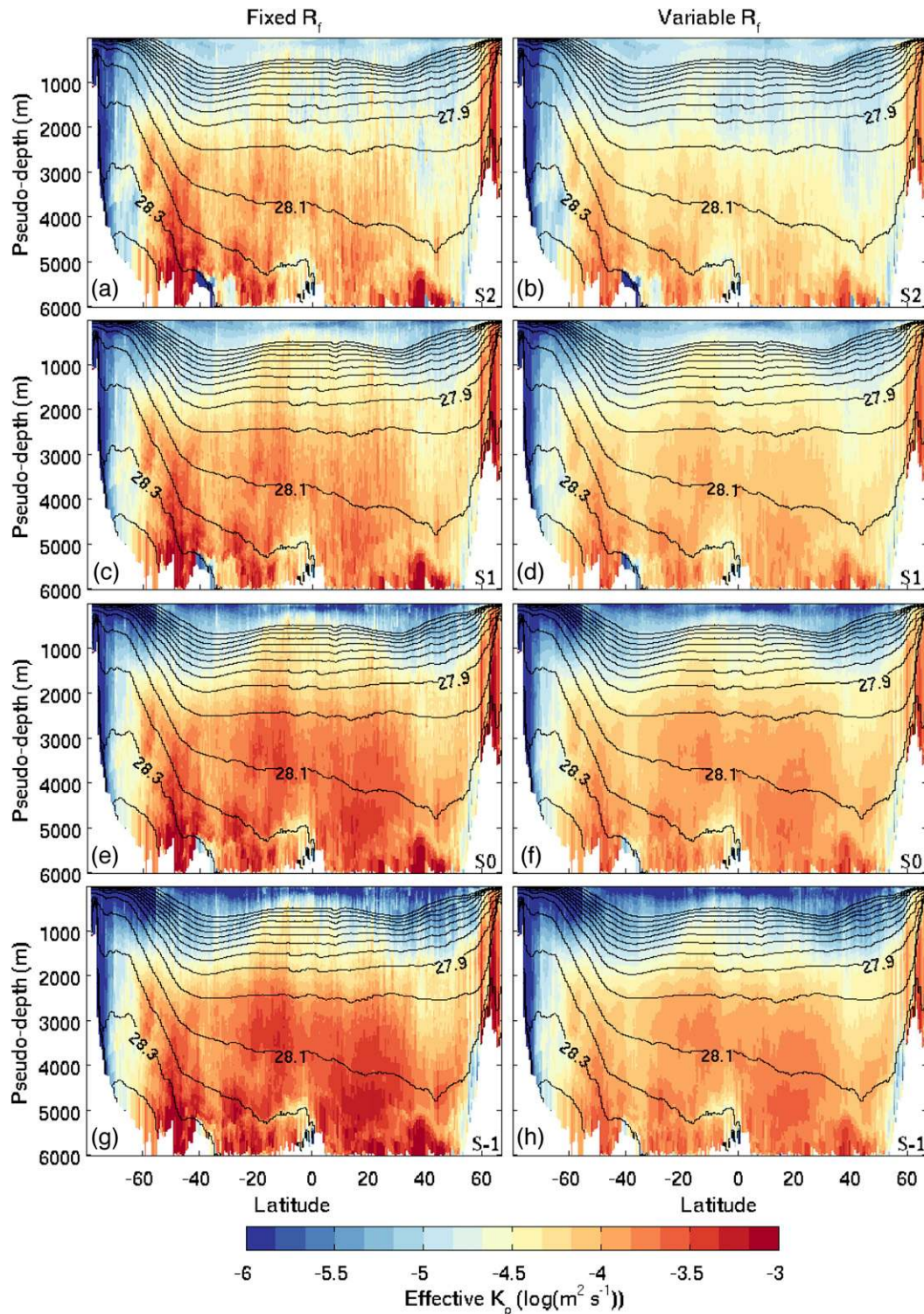


FIG. 4. Effective diffusivity [$\log(\text{m}^2 \text{s}^{-1})$] resulting from near-field and far-field mixing combined, according to (left) fixed and (right) variable efficiency models. Effective diffusivities are calculated as a stratification-weighted mean along isopycnals ($\frac{\int K_p N^2 dS}{\int N^2 dS}$). The vertical structure of remote tidal dissipation is specified according to scenario (a),(b) S2; (c),(d) S1; (e),(f) S0; or (g),(h) S-1. Density-binned values are reprojected to pseudodepth for visual purposes. Neutral density surfaces within 27–28.5 kg m^{-3} are contoured every 0.1 kg m^{-3} .

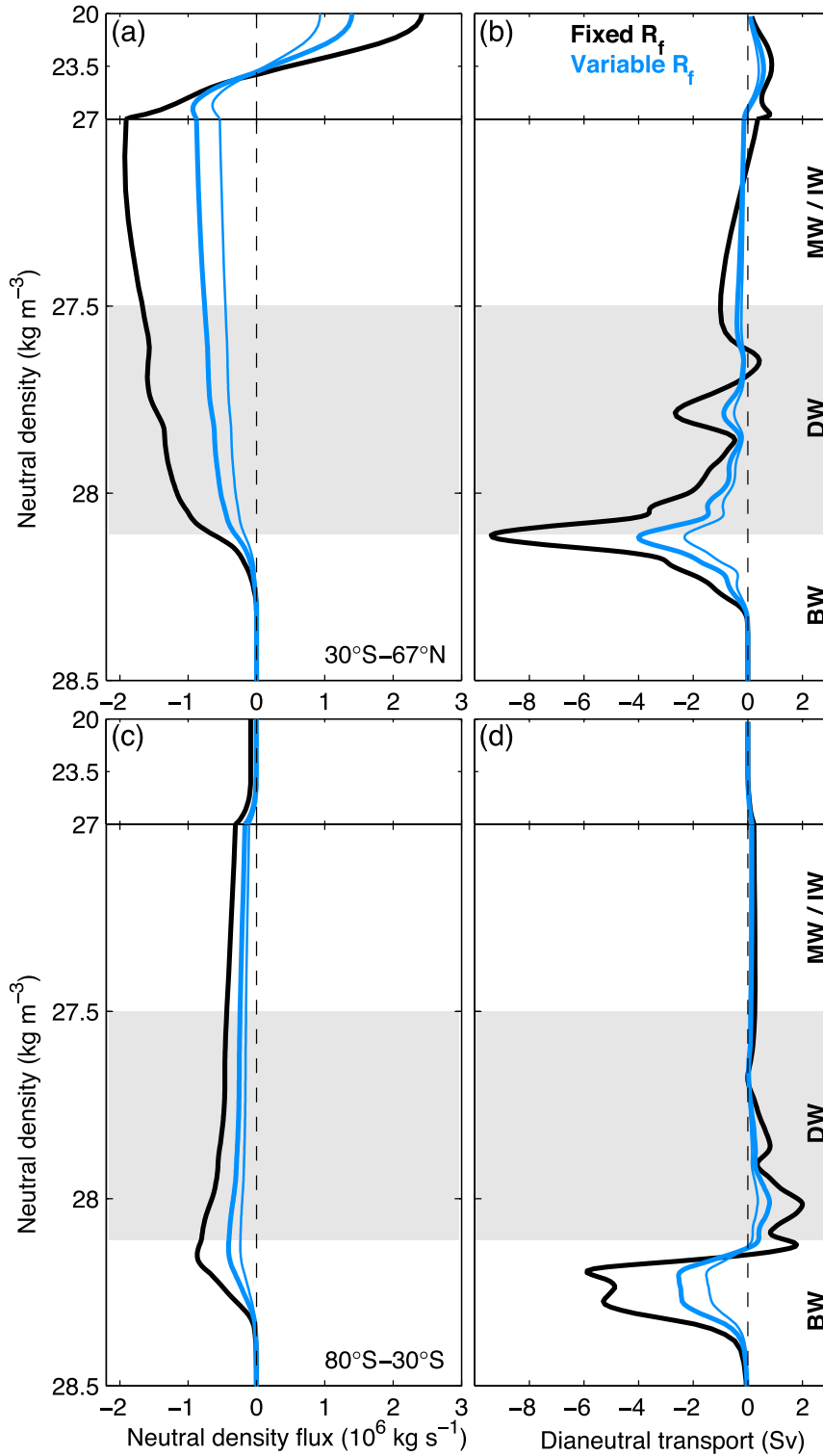


FIG. 5. Water mass transformation by near-field diapycnal mixing for the regions (a),(b) north and (c),(d) south of 30°S . (a),(c) Neutral density fluxes (10^6 kg s^{-1}) and (b),(d) dianeutral transports (Sv) induced by near-field mixing alone under fixed (thick black) and variable (thick blue) R_f . Negative dianeutral transports correspond to upwelling. The thin blue line shows results from an alternative variable R_f formulation, where the lower limit of the energetic regime is set to $\text{Re}_b = 100$ instead of $\text{Re}_b = 400$. Note the different vertical scale above and below $\gamma = 27 \text{ kg m}^{-3}$. Neutral density ranges of bottom (BW), deep (DW), and mode/intermediate (MW/IW) waters are indicated by the light gray shading and the right-end labels.

flow. This is not the case for scenario S2, however, where the added mixing has almost no influence on abyssal waters (Fig. 6 and Table 1). With the addition of remote tidal dissipation under scenario S1 and variable R_f , AABW upwelling north of 30°S is doubled from 4 to 8 Sv, compared to an increase from 9 to 15 Sv assuming a fixed efficiency. Stronger AABW consumption rates of 13 and 15 Sv are achieved with the inclusion of far-field mixing with vertically uniform (S0) or depth-increasing (S-1) dissipation, respectively. Yet these rates remain much weaker than the corresponding 25 and 33 Sv of AABW upwelling that one would infer from a fixed mixing efficiency of one-sixth. These results suggest that internal tides and lee waves generated by tidal and geostrophic flows impinging on rough topography are unlikely to be able to sustain alone the estimated 20–30 Sv of northward bottom water inflow to the Atlantic and Indo-Pacific basins (Ganachaud and Wunsch 2000; Lumpkin and Speer 2007; Talley et al. 2003; Talley 2008, 2013; Naveira Garabato et al. 2014).

Reduced mixing efficiencies at high Re_b also have implications for the local structure of abyssal flows (Fig. 7). Because mixing-induced buoyancy fluxes must vanish at the seafloor to meet a no-flux bottom boundary condition, mixing efficiency must be zero at the seabed. (We note that the downward heat flux actually vanishes very near the seafloor before reversing sign to meet the bottom geothermal flux—a fact ignored here, for it does not affect the present discussion.) Under the assumption of a fixed efficiency, the transition from $R_f = 1/6$ to $R_f = 0$ occurs de facto within the bottom-most grid cell through the enforcement of the no-flux boundary condition for diffusive heat and salt fluxes. In the case of increasing energy dissipation with depth, as parameterized for near-field mixing, this implies that the downward buoyancy flux is divergent throughout the water column except in the deepest grid cell, where all the buoyancy deposition is concentrated. As a result, strong upwelling (defined here as diapycnal transport toward lower densities) at the lowest level contrasts with downwelling in overlying waters (LMSNG). This behavior can be observed in Fig. 7c, where large downward transports near the neutral surface incrop adjoin strong upward transports at the grounding grid cells. In contrast, the $R_f(Re_b)$ model allows a natural transition toward the no-flux bottom boundary condition, with $R_f \rightarrow 0$ as $N^2 \rightarrow 0$. Consequently, the peak buoyancy flux induced by near-field mixing is generally weaker and situated higher up in the water column, and the resulting bottom buoyancy gain is both smaller and distributed over a thicker layer above the seafloor. Upwelling then occurs through weaker velocities over a thicker bottom

layer, and the downward transports above that layer are significantly damped (Figs. 7a–d).

d. Sensitivity to regime limits

Water mass transformation estimates were found to be insensitive to the inclusion of differential diffusion and reduced efficiencies in the buoyancy-controlled regime (not shown): differences between the fixed and variable R_f models presented in Figs. 3–7 are almost entirely attributable to differing mixing efficiencies in the energetic regime. In contrast, sensitivity to the precise formulation of the energetic regime may be expected to be significant. In particular, there remains uncertainty in the validity ranges of the transitional and energetic regimes: whereas field measurements suggest a transition between these regimes close to $Re_b = 400$, numerical work suggested an earlier transition near $Re_b = 100$ (Shih et al. 2005; Bouffard and Boegman 2013).

To examine the sensitivity to this critical level, we repeated the analysis using the more stringent $Re_b = 100$ transition. The energetic regime diffusivity and efficiency are then given by

$$K_p = 2\nu\sqrt{Re_b}, \quad R_f = 1/(1 + 0.5\sqrt{Re_b}). \quad (10)$$

Further reduction of buoyancy fluxes and diapycnal transports was obtained (Figs. 5 and 6, thin blue), with as little as 3–8 Sv of AABW upwelling induced by near-field and far-field mixing combined. Using this formulation, locally dissipating internal waves alone sustain ~2 Sv of AABW flow and supply 26 GW of oceanic potential energy globally. This is about 40% less than the rates inferred from our reference variable R_f formulation, which was shown to be in closer agreement with available field observations (Bouffard and Boegman 2013). Although further observational constraints are thus required to narrow down the uncertainty associated with regime transitions, the sensitivity to the lower limit of the energetic regime is relatively modest compared to the difference between constant and variable efficiency models (Figs. 5 and 6).

4. Implications for the closure of the abyssal overturning

The present water mass transformation estimates show that topographically enhanced mixing driven by breaking of locally generated internal waves is unlikely to sustain more than 5 Sv of Antarctic Bottom Water flow at 30°S, providing for only about a fifth of the estimated strength of the abyssal circulation (Ganachaud and Wunsch 2000; Lumpkin and Speer 2007; Talley et al.

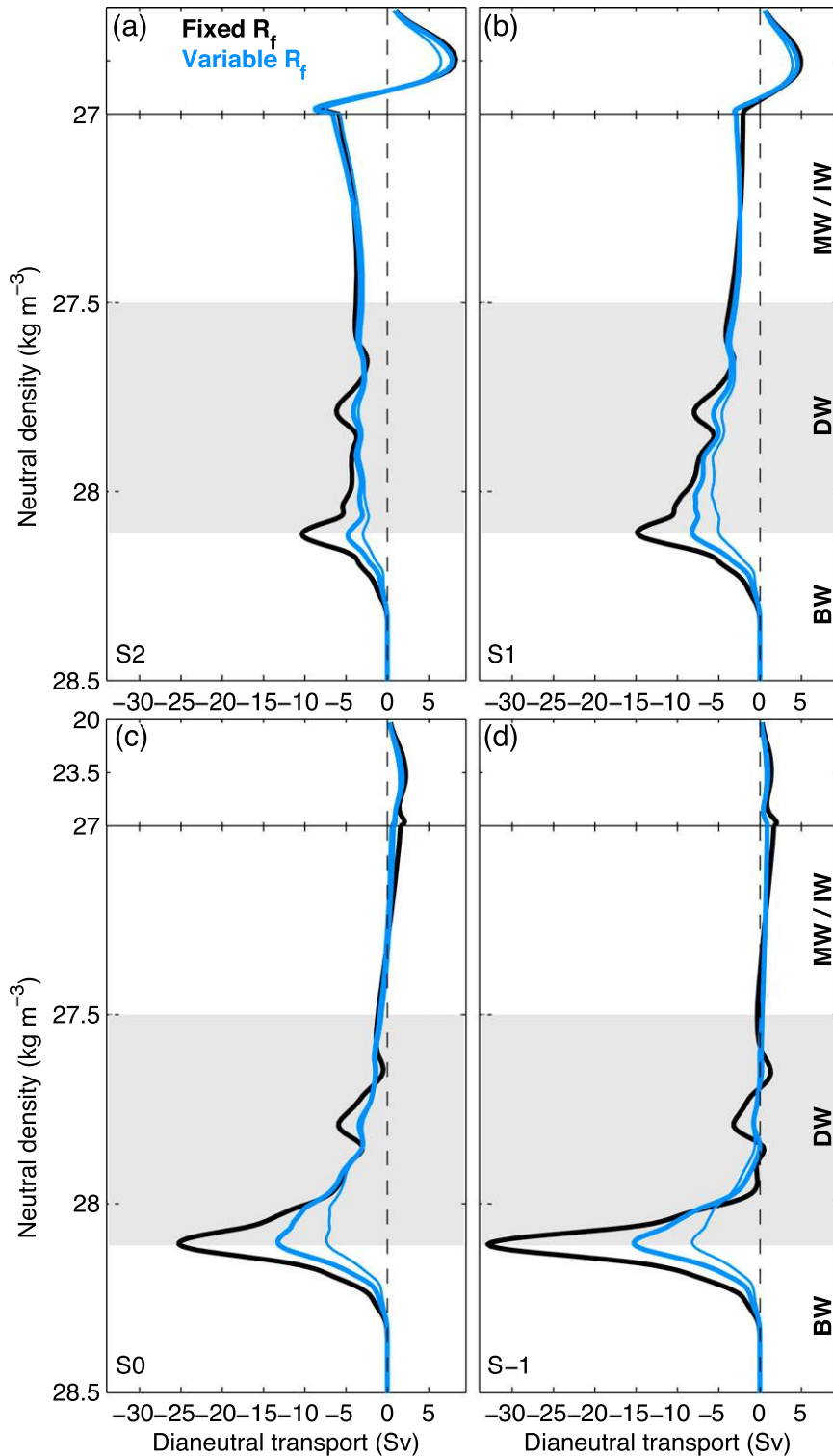


FIG. 6. Dianeutral transports (Sv) induced by near-field and far-field mixing combined within the 30°S – 67°N ocean domain, under fixed (thick black) and variable (thick blue) R_f . The vertical structure of remote energy dissipation scales either as (a) N^2 , (b) N , (c) 1, or (d) N^{-1} . The thin blue line shows results from an alternative variable R_f formulation where the lower limit of the energetic regime occurs at $\text{Re}_b = 100$ instead of $\text{Re}_b = 400$. Note the different vertical scale above and below $\gamma = 27 \text{ kg m}^{-3}$. Neutral density ranges of bottom, deep, and mode/intermediate waters are indicated by the light gray shading and the right-end labels.

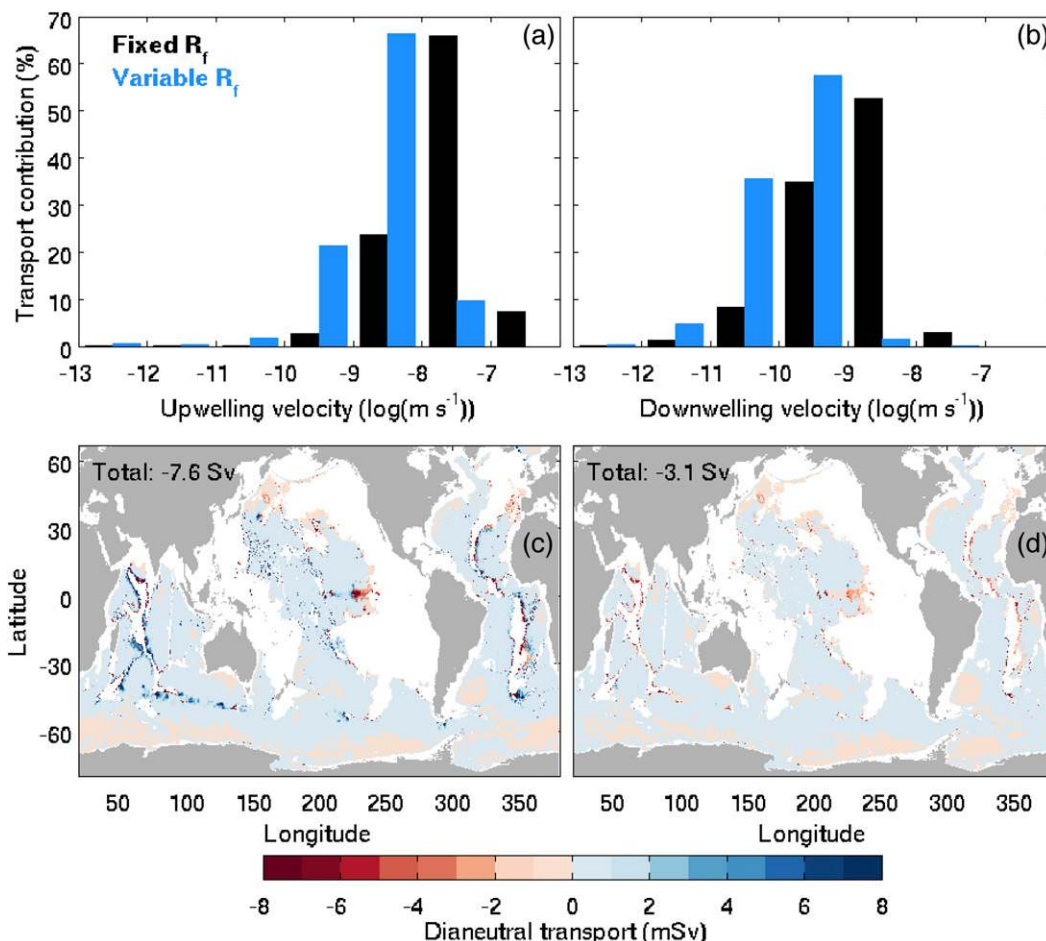


FIG. 7. Impact of mixing efficiency variability on the local structure of dianeutral transports. (a),(b) Contribution of given ranges of dianeutral velocity [$\log(\text{m s}^{-1})$] to overall (a) upward and (b) downward transports under fixed (black) and variable (blue) R_f . (c),(d) Maps of local dianeutral transports (mSv) induced by near-field mixing across the 28.11 kg m^{-3} neutral surface according to (c) fixed and (d) variable R_f models.

2003; Talley 2008, 2013; Naveira Garabato et al. 2014). Radiation of low-mode internal tides, by redistributing internal wave energy over large ocean volumes and powering the background internal wave field, could be a more efficient driver of the abyssal overturning (Oka and Niwa 2013). Indeed, a fairly spread distribution of remote tidal dissipation would allow a larger fraction of the available energy to actually contribute to buoyancy exchange. Yet the amount of buoyancy transferred to abyssal waters is strongly dependent on the vertical structure of far-field dissipation, and little to no impact on the AABW layer is possible if the resultant mixing is mostly confined to the upper ocean. An important portion of the available energy may also be lost at continental margins without contributing to thermocline or deep-water mass transformation (Kelly et al. 2013; Waterhouse et al. 2014). Moreover, even in the highly favorable cases of vertically homogeneous or

depth-increasing energy dissipation, far-field tidal mixing was estimated to contribute no more than 9–11 Sv of additional AABW upwelling.

Hence, taking current best estimates of the strength of the abyssal overturning at face value, we posit that additional sources of buoyancy or mixing are responsible for significant AABW consumption. However, non-linearity of the Re_b -dependent model implies that additional power inputs to the internal wave field will be increasingly inefficient at causing additional mixing, especially if placed in the weakly stratified abyss. In contrast, the weak stratification of relatively light bottom waters ($\gamma \approx 28.11 \text{ kg m}^{-3}$) plays in favor of their consumption by geothermal heating because it enhances the incrop area and thereby the overall heat gain of these neutral density layers (LMSNG). Thus, whereas mixing is more efficient at homogenizing well-stratified water masses, a direct buoyancy supply is more apt at

ultimately consuming well-homogenized waters. Nevertheless, the geothermal circulation, estimated to peak at about 5 Sv across $\gamma \approx 28.11 \text{ kg m}^{-3}$ (Emile-Geay and Madec 2009; LMSNG), is likely insufficient to close the abyssal overturning. Another substantial contribution could be provided by mixing in constricted flows across deep sills, where strong shear, hydraulic jumps, and entrainment in descending plumes can cause much more intense mixing than the turbulence driven by instability of the internal wave field. Indeed, overflow-related mixing in major interbasin passages (Polzin et al. 1996; Bryden and Nurser 2003) or in small but widespread canyons cutting across ridge flanks and shelf slopes (Thurnherr and Speer 2003; Thurnherr et al. 2005) has been suggested to be an important actor of AABW transformation. In such deep overflows, concentrated yet highly efficient mixing is tenable because the swift, continuous inflow of dense waters maintains large density gradients.

We note that geothermal heating and internal wave breaking, by forcing upwelling along the bottom topography (St. Laurent et al. 2001; LMSNG), could contribute to drive the up-valley canyon flows suspected to trigger significant mixing downstream of canyon sills (Thurnherr et al. 2005). Nonetheless, the energy required to sustain passage flows and the associated mixing likely originates to a large extent in the surface, large-scale wind and buoyancy forcing of the general circulation (Hughes and Griffiths 2006; Hughes et al. 2009; Saenz et al. 2012). Except for the relatively small fraction of the large-scale wind work dissipated by lee-wave generation (Naveira Garabato et al. 2013), these forcings are absent from our calculations, which only include the breaking of lee and tidally forced internal waves as a direct mixing source.

To illustrate the inability of energy sources considered in this study to match bulk observational estimates of deep ocean mixing levels, we compute effective neutral density diffusivities as $\iint_{\gamma} F_{\text{eq}}^{\gamma} dS / \iint_{\gamma} \partial_z \gamma dS$, restricted to the 32°S–48°N region, and plot the corresponding profiles of effective K_{γ} against the analogous inverse estimate of Lumpkin and Speer (2007) (Fig. 8). Using this definition of effective K_{γ} and a map of geothermal heat fluxes (Goutorbe et al. 2011), the contribution of geothermal heating can be incorporated in a fashion consistent to that of diapycnal mixing (LMSNG). Because the observationally based profile should reflect all processes affecting the inversed hydrographic properties, and since geothermal heating was shown to drive significant AABW consumption, we include its contribution here. When accounting for R_f variability, the envelope of effective diffusivities associated with the four tested scenarios remains well below the

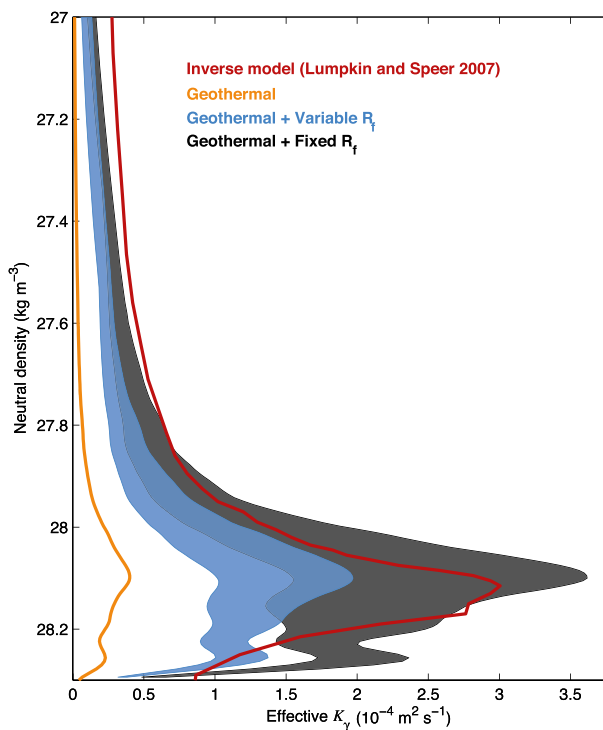


FIG. 8. Profiles of effective neutral density diffusivity ($10^{-4} \text{ m}^2 \text{ s}^{-1}$) for the 32°S–48°N region. The effective K_{γ} is calculated as $\iint_{\gamma} F_{\text{eq}}^{\gamma} dS / \iint_{\gamma} \partial_z \gamma dS$. Effective diffusivities resulting from geothermal heating, near-field mixing and far-field mixing combined are shown for fixed (black) and variable (blue) R_f models, where the envelopes encompass the range of scenarios S2 to S–1. The contribution of geothermal heating alone (orange) and the inverse estimate of Lumpkin and Speer (2007) (red) are plotted. Data for the observationally based estimate obtained courtesy of R. Lumpkin.

observationally based estimate. With a fixed efficiency, effective diffusivities are significantly larger but also fall short of the inverse estimate at most levels under scenarios S2, S1, and S0. Interestingly, the mismatch is not only significant at abyssal levels but also at lighter densities throughout the range of deep, mode, and intermediate waters. The lack of mixing at these densities is suggestive of missing energy sources for the internal wave field, such as wind-generated near-inertial waves (Alford 2003; Rimac et al. 2013). Mixing in narrow passages at ridge crests could also provide for some of the missing deep-water transformation (Thurnherr 2006; St. Laurent and Thurnherr 2007). But given that AABW covers about two-thirds of the ocean floor (Johnson 2008), such boundary processes are expected to have a much more prominent role at abyssal densities.

Some clues as to which processes may supplement AABW consumption can be obtained by decomposing water mass transformation rates between the Indian, Pacific, and Atlantic basins (Table 2). Maximum

TABLE 2. Maximum abyssal upwelling rates (Sv) by basin as compared to the range of estimates from hydrographic inversions. Herein-estimated AABW upwelling rates correspond to the combined effect of near-field mixing, far-field mixing and geothermal heating. Scenarios used for the distribution of far-field dissipation are indicated in the top row. Considered observationally based estimates are referenced in the text.

	S2	S1	S0	S-1	Inverse estimates
30°S–67°N	10	13	18	20	20–30
Pacific	6	7	10	11	7–14
Atlantic	3	3	5	5	4–8
Indian	2	3	4	4	9–18

upwelling rates induced by near-field mixing, far-field mixing, and geothermal heating combined under variable R_f are indicated for all three basins, restricted to the region north of 30°S. Note that peak upwelling concurs with the peak incrop area for each basin and occurs at a slightly denser level in the Indian Ocean (28.14 kg m^{-3}) than in the other two basins (28.11 kg m^{-3}). Strikingly, the Indian Ocean also stands out when the presently estimated AABW consumption rates are compared to the approximate range of observational estimates for the strength of basin overturnings (Ganachaud and Wunsch 2000; Talley et al. 2003; Lumpkin and Speer 2007; Talley 2008, 2013). Although the Atlantic and Pacific AABW transports tend to lie on the low side of observational ranges, the discrepancy is much more pronounced in the Indian Ocean, for which all scenarios clearly fall short of the 9–18 Sv of overturning indicated by inverse estimates. Breaking internal waves in the ocean interior and geothermal heating appear unable to explain the disproportionate amount of AABW inflow to the Indian Ocean (Huussen et al. 2012; Decloedt and Luther 2012): its comparatively small area and incrop areas (not shown) would require unobserved, exceptionally strong internal wave activity or geothermal heat fluxes to sustain its strong abyssal circulation. Huussen et al. (2012) suggested that near-boundary mixing, likely concentrated in fracture zones and interbasin passages (MacKinnon et al. 2008), may instead provide for the required intense AABW transformation. Support for this hypothesis comes notably from the particularly dense network of ridges and fracture zones, the numerous subbasins (see Figs. 7c,d), and the high average abyssal hill roughness that characterize the Indian Ocean bathymetry (Goff and Arbic 2010; Huussen et al. 2012).

5. Conclusions

A recent turbulent diffusivity model that accounts for reduced mixing efficiencies in actively mixing waters was used to revise estimates of water mass

transformation by breaking internal tides and lee waves. The variable R_f model led to a 50%–60% reduction of the global potential energy source and AABW upwelling rate attributable to lee-wave radiation and near-field tidal mixing taken in isolation. Indeed, mixing efficiency tends to be low in regions of enhanced internal wave breaking near rough topography, where intense turbulence rapidly erodes the near-bottom stratification, reducing its ability to sustain buoyancy fluxes. With only about 4 Sv of AABW consumption and 45 GW of global potential energy supply, the overall contribution of parameterized near-field mixing to the maintenance of the abyssal stratification is found to be comparable to that of geothermal heating.

To explore the potential importance of varying mixing efficiencies for remotely dissipating internal tides, we specified four idealized distributions of remote tidal dissipation: the available power was horizontally spread around generation sites and distributed in the vertical by assuming that energy dissipation scales with N^2 , N , 1, or N^{-1} . Rather than realistic parameterizations of remote energy dissipation, these idealized scenarios are meant to achieve preliminary understanding and to provide probable bounds on water mass transformation by far-field tidal mixing. The addition of far-field energy dissipation raises the AABW consumption rate to 5–15 Sv and the potential energy supply to 107–134 GW, compared to 10–33 Sv and 161–231 GW under the traditional assumption of a fixed efficiency, where the ranges encompass the four tested vertical structures. Thus, whether low-mode internal tides tend to cause mixing in the pycnocline away from AABW or in weakly stratified abyssal waters, breaking lee waves and internal tides appear unable to sustain alone a 20–30-Sv abyssal overturning.

The important role of variability in mixing efficiency for deep-water mass transformation and ocean energetics implies that the common assumption of a constant efficiency of 17%–20% should be abandoned for more consistent formulations, such as the Re_b -dependent model employed here (Shih et al. 2005; Bouffard and Boegman 2013). In particular, the $R_f(Re_b)$ model is suitable for inclusion in mixing parameterizations of ocean models that infer diapycnal diffusivities from energy dissipation rates (St. Laurent et al. 2002; Polzin 2009; Ollers and Eden 2013). Its implementation will obviate the need to impose an arbitrary minimum on stratification when deducing K_ρ from N^2 and ε_T (Simmons et al. 2004; Oka and Niwa 2013) and will strongly reduce sensitivity to the chosen upper bound on K_ρ . Moreover, it will allow the buoyancy flux to naturally satisfy the no-flux bottom boundary condition (e.g., Melet et al. 2013a).

TABLE A1. Parameterization of the diapycnal heat diffusivity. The top two rows describe the Re_b -dependent formulation of Bouffard and Boegman (2013). The bottom two rows indicate ranges and equations used in the present implementation. The indicated upper limits of the energetic regime correspond to the imposed upper-bound on K_Θ , taken as $10^{-2} \text{ m}^2 \text{ s}^{-1}$.

Regime	Molecular	Buoyancy controlled	Transitional	Energetic
Re_b (range)	[0; 1.7]	[1.7; 8.5]	[8.5; 400]	[400; 6.25×10^6]
$K_\Theta(\text{Re}_b)$ ($\text{m}^2 \text{ s}^{-1}$)	1.4×10^{-7}			
Re_b^T (range)	[0; 1.93]	[1.93; 10.2]	[10.2; 480]	[480; 7.50×10^7]
$K_\Theta(\text{Re}_b^T)$ ($\text{m}^2 \text{ s}^{-1}$)	1.4×10^{-7}			

Although this Re_b -dependent parameterization has been shown to be consistent with available numerical, experimental, and field data (Bouffard and Boegman 2013), including Brazil basin observations (Ledwell et al. 2000), significant uncertainty remains in the exact definition of the different regimes. Because decreased mixing efficiencies and differential diffusion at low turbulence intensities have a minimal impact on large-scale transformation by internal wave-driven mixing, only uncertainty at relatively high Re_b is of concern here. We tested an alternative variable R_f formulation where the shift from the transitional to the energetic regime occurs at a lower Re_b level. This formulation, which agrees more closely with numerical results (Shih et al. 2005) but less so with field measurements (Bouffard and Boegman 2013), leads to even stronger reductions of potential energy input and AABW consumption by internal wave breaking, with near-field and far-field mixing together contributing 3–8 Sv of AABW upwelling north of 30°S. The sensitivity to this critical Re_b highlights the need to reduce uncertainties associated with validity ranges of the high-diffusivity regimes. Targeted field measurements (e.g., Bluteau et al. 2013) are required to further constrain the Re_b dependence of mixing efficiency in strongly mixing waters and to critically examine the model's limitations across a range of oceanic conditions and scales.

Local oceanic mixing efficiencies likely depend on the specific flow instabilities through which energy cascades to the dissipation scale, and the time–space intermittency of turbulence implies that they must vary on short spatial and temporal scales (Smyth et al. 2001; Ivey et al. 2008; Mashayek et al. 2013; Mashayek and Peltier 2013). Ocean general circulation models do not resolve the turbulent cascade and require parameterizations that realistically incorporate the large-scale statistics of irreversible mixing (Arneborg 2002). Although the universality of the proposed Re_b regimes is debatable (e.g., Mater and Venayagamoorthy 2014), it is argued that the $R_f(\text{Re}_b)$ model improves upon the constant efficiency assumption by capturing some of the statistical variability of oceanic mixing efficiency, in accord with observations and theory (Bouffard and Boegman 2013). Implementation of the Re_b -dependent parameterization, together with efforts to refine and generalize the model by factoring in the

process and scale dependence of mixing efficiency, should therefore contribute to improve the representation of diapycnal mixing in ocean models.

Acknowledgments. We are grateful to F. Roquet and A. Melet for sharing the datasets of the energy flux into internal tides of Nycander (2005) and Melet et al. (2013b). We also thank R. Lumpkin for providing data from his inverse solution and J.-B. Sallée for helpful comments on the manuscript. Suggestions from two anonymous reviewers helped to substantially improve the manuscript. This work was undertaken as part of the EMBRACE project, funded by the European Union's Seventh Framework Programme under Grant Agreement 282672.

APPENDIX

Implementation of the Turbulent Diffusivity Model

The turbulent diffusivity (Shih et al. 2005; Bouffard and Boegman 2013) and diffusivity ratio (Jackson and Rehmann 2014) parameterizations considered in this study are both expressed as a function of the turbulence intensity parameter $\text{Re}_b = \varepsilon_\nu / (\nu N^2)$. Although frictional dissipation ε_ν is the most readily accessible quantity from observations in the field, mixing parameterizations for ocean models are formulated upon the energy lost to the internal wave field, $\varepsilon_T = \varepsilon_\nu + K_\rho N^2$. To reframe the model equations in terms of ε_T rather than ε_ν , we first define a modified turbulence intensity parameter $\text{Re}_b^T = \varepsilon_T / (\nu N^2) = \text{Re}_b + (K_\rho / \nu)$. The Re_b^T -dependent formulation can then be obtained by substituting $\text{Re}_b^T - (K_\rho / \nu)$ for Re_b in $K_\rho(\text{Re}_b)$ equations and solving for K_ρ . This is easily done for the transitional and energetic regimes:

$$\text{Transitional } (10.2 \leq \text{Re}_b^T \leq 480): K_\rho = \frac{1}{6} \nu \text{Re}_b^T \quad \text{and} \quad (\text{A1})$$

$$\text{Energetic } (480 \leq \text{Re}_b^T): K_\rho = 4\nu(\sqrt{4 + \text{Re}_b^T} - 2). \quad (\text{A2})$$

No simple analytical solution can be obtained for the buoyancy-controlled regime, however. Given the inherent

degree of uncertainty in the exponents and coefficients of the Bouffard and Boegman (2013) experimental fits, we deem it justified to simplify Re_b^T -dependent equations in the buoyancy-controlled and energetic regimes by using expressions of the form $K_\rho = C\nu(Re_b^T)^n$, where the exponent n is kept the same as in the original Re_b -based fits, and the nondimensional constant C is adjusted to respect both continuity and the limits of the transitional regime (Table A1). This simplification conserves the general behavior of the energetic regime, and the resulting K_ρ deviates by less than 10% from that given by (A2). Note that the difference between heat and density diffusivities at low Re_b complicates in principle the reformulation of K_θ in the buoyancy-controlled regime, but such complications can be ignored in view of the above-mentioned uncertainty, especially in this weak diffusivity regime.

The salt diffusivity is then deduced from $K_\theta(Re_b^T)$ using the diffusivity ratio parameterized by Jackson and Rehmann (2014):

$$K_{S_A}/K_\theta = \frac{1.01}{2} + \frac{0.99}{2} \tanh \left\{ 0.92 \left[\log \left(\frac{5}{6} Re_b^T \right) - 0.60 \right] \right\}, \quad (A3)$$

where the original equation was simply modified by replacing Re_b with $(5/6)Re_b^T$. This modification introduces a slight distortion of the original fit outside of the transitional regime but preserves the exact Re_b dependence within $8.5 \leq Re_b \leq 400$. Again, this necessary adjustment is deemed well within the uncertainty of the parameterization.

REFERENCES

- Alford, M. H., 2003: Improved global maps and 54-year history of wind-work on ocean inertial motions. *Geophys. Res. Lett.*, **30**, 1424, doi:10.1029/2002GL016614.
- Arneborg, L., 2002: Mixing efficiencies in patchy turbulence. *J. Phys. Oceanogr.*, **32**, 1496–1506, doi:10.1175/1520-0485(2002)032<1496:MEIPT>2.0.CO;2.
- , and B. Liljebladh, 2001: The internal seiches in Gullmar Fjord. Part II: Contribution to basin water mixing. *J. Phys. Oceanogr.*, **31**, 2567–2574, doi:10.1175/1520-0485(2001)031<2567:TISIGF>2.0.CO;2.
- Barry, M. E., G. N. Ivey, K. B. Winters, and J. Imberger, 2001: Measurements of diapycnal diffusivities in stratified fluids. *J. Fluid Mech.*, **442**, 267–291, doi:10.1017/S0022112001005080.
- Bluteau, C. E., N. L. Jones, and G. N. Ivey, 2013: Turbulent mixing efficiency at an energetic ocean site. *J. Geophys. Res.*, **118**, 4662–4672, doi:10.1002/jgrc.20292.
- Bouffard, D., and L. Boegman, 2013: A diapycnal diffusivity model for stratified environmental flows. *Dyn. Atmos. Oceans*, **61**–**62**, 14–34, doi:10.1016/j.dynatmoce.2013.02.002.
- Bryan, K., and L. J. Lewis, 1979: A water mass model of the World Ocean. *J. Geophys. Res.*, **84**, 2503–2517, doi:10.1029/JC084iC05p02503.
- Bryden, H. L., and A. J. G. Nurser, 2003: Effects of strait mixing on ocean stratification. *J. Phys. Oceanogr.*, **33**, 1870–1872, doi:10.1175/1520-0485(2003)033<1870:EOSMOO>2.0.CO;2.
- Davis, K. A., and S. G. Monismith, 2011: The modification of bottom boundary layer turbulence and mixing by internal waves shoaling on a barrier reef. *J. Phys. Oceanogr.*, **41**, 2223–2241, doi:10.1175/2011JPO4344.1.
- de Lavergne, C., G. Madec, J. Le Sommer, A. J. G. Nurser, and A. C. Naveira Garabato, 2015: On the consumption of Antarctic Bottom Water in the abyssal ocean. *J. Phys. Oceanogr.*, **46**, 635–651, doi:10.1175/JPO-D-14-0201.1.
- de Young, B., and S. Pond, 1989: Partition of energy loss from the barotropic tide in fjords. *J. Phys. Oceanogr.*, **19**, 246–252, doi:10.1175/1520-0485(1989)019<0246:POELFT>2.0.CO;2.
- Delcloedt, T., and D. S. Luther, 2012: Spatially heterogeneous diapycnal mixing in the abyssal ocean: A comparison of two parameterizations to observations. *J. Geophys. Res.*, **117**, C11025, doi:10.1029/2012JC008304.
- Dunckley, J. F., J. R. Koseff, J. V. Steinbeck, S. G. Monismith, and A. Genin, 2012: Comparison of mixing efficiency and vertical diffusivity models from temperature microstructure. *J. Geophys. Res.*, **117**, C10008, doi:10.1029/2012JC007967.
- Eden, C., and D. Olbers, 2014: An energy compartment model for propagation, nonlinear interaction, and dissipation of internal gravity waves. *J. Phys. Oceanogr.*, **44**, 2093–2106, doi:10.1175/JPO-D-13-0224.1.
- Emile-Geay, J., and G. Madec, 2009: Geothermal heating, diapycnal mixing and the abyssal circulation. *Ocean Sci.*, **5**, 203–217, doi:10.5194/os-5-203-2009.
- Ganachaud, A., and C. Wunsch, 2000: Improved estimates of global ocean circulation, heat transport and mixing from hydrographic data. *Nature*, **408**, 453–457, doi:10.1038/35044048.
- Gargett, A. E., 1984: Vertical eddy diffusivity in the ocean interior. *J. Mar. Res.*, **42**, 359–393, doi:10.1357/002224084788502756.
- Gloor, M., A. Wüest, and D. M. Imboden, 2000: Dynamics of mixed bottom boundary layers and its implications for diapycnal transport in a stratified, natural water basin. *J. Geophys. Res.*, **105**, 8629–8646, doi:10.1029/1999JC900303.
- Goff, J. A., and B. K. Arbic, 2010: Global prediction of abyssal hill roughness statistics for use in ocean models from digital maps of paleo-spreading rate, paleo-ridge orientation, and sediment thickness. *Ocean Modell.*, **32**, 36–43, doi:10.1016/j.ocemod.2009.10.001.
- Gouretski, V. V., and K. P. Koltermann, 2004: WOCE global hydrographic climatology. Bundesamt für Seeschifffahrt und Hydrographie Tech. Rep. 35, 52 pp. [Available online at http://odv.awi.de/fileadmin/user_upload/odv/data/Gouretski-Koltermann-2004/BSH35_report_final.pdf.]
- Goutorbe, B., J. Poort, F. Lucazeau, and S. Raillard, 2011: Global heat flow trends resolved from multiple geological and geophysical proxies. *Geophys. J. Int.*, **187**, 1405–1419, doi:10.1111/j.1365-246X.2011.05228.x.
- Holt, S. E., J. R. Koseff, and J. H. Ferziger, 1992: A numerical study of the evolution and structure of homogenous stably stratified sheared turbulence. *J. Fluid Mech.*, **237**, 499–539, doi:10.1017/S0022112092003513.
- Huang, R. X., 1999: Mixing and energetics of the oceanic thermohaline circulation. *J. Phys. Oceanogr.*, **29**, 727–746, doi:10.1175/1520-0485(1999)029<0727:MAEOTO>2.0.CO;2.
- Hughes, G. O., and R. W. Griffiths, 2006: A simple convective model of the global overturning circulation, including effects

- of entrainment into sinking regions. *Ocean Modell.*, **12**, 46–79, doi:10.1016/j.ocemod.2005.04.001.
- , A. M. Hogg, and R. W. Griffiths, 2009: Available potential energy and irreversible mixing in the meridional overturning circulation. *J. Phys. Oceanogr.*, **39**, 3130–3146, doi:10.1175/2009JPO4162.1.
- Hult, E. L., C. D. Troy, and J. R. Koseff, 2011: The mixing efficiency of interfacial waves breaking at a ridge: 1. Overall mixing efficiency. *J. Geophys. Res.*, **116**, C02003, doi:10.1029/2010JC006485.
- Huussen, T. N., A. C. Naveira Garabato, H. L. Bryden, and E. L. McDonagh, 2012: Is the deep Indian Ocean MOC sustained by breaking internal waves? *J. Geophys. Res.*, **117**, C08024, doi:10.1029/2012JC008236.
- Inall, M. E., 2009: Internal wave induced dispersion and mixing on a sloping boundary. *Geophys. Res. Lett.*, **36**, L05604, doi:10.1029/2008GL036849.
- Iudicone, D., G. Madec, B. Blanke, and S. Speich, 2008a: The role of Southern Ocean surface forcings and mixing in the global conveyor. *J. Phys. Oceanogr.*, **38**, 1377–1400, doi:10.1175/2008JPO3519.1.
- , —, and T. J. McDougall, 2008b: Water-mass transformations in a neutral density framework and the key role of light penetration. *J. Phys. Oceanogr.*, **38**, 1357–1376, doi:10.1175/2007JPO3464.1.
- Ivey, G. N., K. B. Winters, and J. R. Koseff, 2008: Density stratification, turbulence, but how much mixing? *Annu. Rev. Fluid Mech.*, **40**, 169–184, doi:10.1146/annurev.fluid.39.050905.110314.
- Jackett, D. R., and T. J. McDougall, 1997: A neutral density variable for the world's oceans. *J. Phys. Oceanogr.*, **27**, 237–263, doi:10.1175/1520-0485(1997)027<0237:ANDVFT>2.0.CO;2.
- Jackson, P. R., and C. R. Rehmann, 2003: Laboratory measurements of differential diffusion in a diffusively stable, turbulent flow. *J. Phys. Oceanogr.*, **33**, 1592–1603, doi:10.1175/2405.1.
- , and —, 2014: Experiments on differential scalar mixing in turbulence in a sheared, stratified flow. *J. Phys. Oceanogr.*, **44**, 2661–2680, doi:10.1175/JPO-D-14-0027.1.
- Johnson, G. C., 2008: Quantifying Antarctic Bottom Water and North Atlantic Deep Water volumes. *J. Geophys. Res.*, **113**, C05027, doi:10.1029/2007JC004477.
- Kelly, S. M., N. L. Jones, J. D. Nash, and A. F. Waterhouse, 2013: The geography of semidiurnal mode-1 internal-tide energy loss. *Geophys. Res. Lett.*, **40**, 4689–4693, doi:10.1002/grl.50872.
- Klocker, A., and T. J. McDougall, 2010: Influence of the nonlinear equation of state on global estimates of diapycnal advection and diffusion. *J. Phys. Oceanogr.*, **40**, 1690–1709, doi:10.1175/2010JPO4303.1.
- Ledwell, J. R., A. J. Watson, and C. S. Law, 1998: Mixing of a tracer in the pycnocline. *J. Geophys. Res.*, **103**, 21 499–21 529, doi:10.1029/98JC01738.
- , E. T. Montgomery, K. L. Polzin, L. C. St. Laurent, R. W. Schmitt, and J. M. Toole, 2000: Evidence for enhanced mixing over rough topography in the abyssal ocean. *Nature*, **403**, 179–182, doi:10.1038/35003164.
- Lumpkin, R., and K. Speer, 2007: Global ocean meridional overturning. *J. Phys. Oceanogr.*, **37**, 2550–2562, doi:10.1175/JPO3130.1.
- MacKinnon, J. A., T. M. S. Johnston, and R. Pinkel, 2008: Strong transport and mixing of deep water through the Southwest Indian Ridge. *Nat. Geosci.*, **1**, 755–758, doi:10.1038/ngeo340.
- , M. H. Alford, R. Pinkel, J. Klymak, and Z. Zhao, 2013: The latitudinal dependence of shear and mixing in the Pacific transiting the critical latitude for PSI. *J. Phys. Oceanogr.*, **43**, 3–16, doi:10.1175/JPO-D-11-0107.1.
- Mashayek, A., and W. R. Peltier, 2013: Shear-induced mixing in geophysical flows: Does the route to turbulence matter to its efficiency? *J. Fluid Mech.*, **725**, 216–261, doi:10.1017/jfm.2013.176.
- , C. P. Caulfield, and W. R. Peltier, 2013: Time-dependent, non-monotonic mixing in stratified turbulent shear flows: implications for oceanographic estimates of buoyancy flux. *J. Fluid Mech.*, **736**, 570–593, doi:10.1017/jfm.2013.551.
- Mater, B. D., and S. K. Venayagamoorthy, 2014: The quest for an unambiguous parameterization of mixing efficiency in stably stratified geophysical flows. *Geophys. Res. Lett.*, **41**, 4646–4653, doi:10.1002/2014GL060571.
- Melet, A., R. Hallberg, S. Legg, and K. L. Polzin, 2013a: Sensitivity of the ocean state to the vertical distribution of internal tide-driven mixing. *J. Phys. Oceanogr.*, **43**, 602–615, doi:10.1175/JPO-D-12-055.1.
- , M. Nikurashin, C. Muller, S. Falahat, J. Nycander, P. G. Timko, B. K. Arbic, and J. A. Goff, 2013b: Internal tide generation by abyssal hills using analytical theory. *J. Geophys. Res.*, **118**, 6303–6318, doi:10.1002/2013JC009212.
- Merryfield, W. J., 2005: Dependence of differential mixing on N and R_p . *J. Phys. Oceanogr.*, **35**, 991–1003, doi:10.1175/JPO2747.1.
- Munk, W. H., 1966: Abyssal recipes. *Deep-Sea Res. Oceanogr. Abstr.*, **13**, 707–730, doi:10.1016/0011-7471(66)90602-4.
- , and C. Wunsch, 1998: Abyssal recipes II: Energetics of tidal and wind mixing. *Deep-Sea Res.*, **45**, 1977–2010, doi:10.1016/S0967-0637(98)00070-3.
- Naveira Garabato, A. C., A. J. G. Nurser, R. B. Scott, and J. A. Goff, 2013: The impact of small-scale topography on the dynamical balance of the ocean. *J. Phys. Oceanogr.*, **43**, 647–668, doi:10.1175/JPO-D-12-056.1.
- , A. P. Williams, and S. Bacon, 2014: The three-dimensional overturning circulation of the Southern Ocean during the WOCE era. *Prog. Oceanogr.*, **120**, 41–78, doi:10.1016/j.pocean.2013.07.018.
- Nikurashin, M., R. Ferrari, N. Grisouard, and K. L. Polzin, 2014: The impact of finite-amplitude bottom topography on internal wave generation in the Southern Ocean. *J. Phys. Oceanogr.*, **44**, 2938–2950, doi:10.1175/JPO-D-13-0201.1.
- Niwa, Y., and T. Hibiya, 2011: Estimation of baroclinic tide energy available for deep ocean mixing based on three-dimensional global numerical simulations. *J. Oceanogr.*, **67**, 493–502, doi:10.1007/s10872-011-0052-1.
- Nycander, J., 2005: Generation of internal waves in the deep ocean by tides. *J. Geophys. Res.*, **110**, C10028, doi:10.1029/2004JC002487.
- Oka, A., and Y. Niwa, 2013: Pacific deep circulation and ventilation controlled by tidal mixing away from the sea bottom. *Nat. Commun.*, **4**, 2419, doi:10.1038/ncomms3419.
- Olbers, D., and C. Eden, 2013: A global model for the diapycnal diffusivity induced by internal gravity waves. *J. Phys. Oceanogr.*, **43**, 1759–1779, doi:10.1175/JPO-D-12-0207.1.
- Osborn, T. R., 1980: Estimates of the local rate of vertical diffusion from dissipation measurements. *J. Phys. Oceanogr.*, **10**, 83–89, doi:10.1175/1520-0485(1980)010<0083:EOTLRO>2.0.CO;2.
- Polzin, K. L., 2009: An abyssal recipe. *Ocean Modell.*, **30**, 298–309, doi:10.1016/j.ocemod.2009.07.006.
- , K. G. Speer, J. M. Toole, and R. W. Schmitt, 1996: Intense mixing of Antarctic Bottom Water in the equatorial Atlantic Ocean. *Nature*, **380**, 54–57, doi:10.1038/380054a0.

- Rehmann, C. R., and J. R. Koseff, 2004: Mean potential energy change in stratified grid turbulence. *Dyn. Atmos. Oceans*, **37**, 271–294, doi:10.1016/j.dynatmoce.2003.09.001.
- Rimac, A., J.-S. von Storch, C. Eden, and H. Haak, 2013: The influence of high-resolution wind stress field on the power input to near-inertial motions in the ocean. *Geophys. Res. Lett.*, **40**, 4882–4886, doi:10.1002/grl.50929.
- Ruddick, B., D. Walsh, and N. Oakey, 1997: Variations in apparent mixing efficiency in the North Atlantic Central Water. *J. Phys. Oceanogr.*, **27**, 2589–2605, doi:10.1175/1520-0485(1997)027<2589:VIAMEI>2.0.CO;2.
- Saenz, J. A., A. M. Hogg, G. O. Hughes, and R. W. Griffiths, 2012: Mechanical power input from buoyancy and wind to the circulation in an ocean model. *Geophys. Res. Lett.*, **38**, L13605, doi:10.1029/2012GL052035.
- Scott, R. B., J. A. Goff, A. C. Naveira Garabato, and A. J. G. Nurser, 2011: Global rate and spectral characteristics of internal gravity wave generation by geostrophic flow over topography. *J. Geophys. Res.*, **116**, C09029, doi:10.1029/2011JC007005.
- Sheen, K. L., and Coauthors, 2013: Rates and mechanisms of turbulent dissipation and mixing in the Southern Ocean: Results from the Diapycnal and Isopycnal Mixing Experiment in the Southern Ocean (DIMES). *J. Geophys. Res.*, **118**, 2774–2792, doi:10.1002/jgrc.20217.
- Shih, L. H., J. R. Koseff, G. N. Ivey, and J. H. Ferziger, 2005: Parameterization of turbulent fluxes and scales using homogeneous sheared stably stratified turbulence simulations. *J. Fluid Mech.*, **525**, 193–214, doi:10.1017/S0022112004002587.
- Simmons, H. L., S. R. Jayne, L. C. St. Laurent, and A. J. Weaver, 2004: Tidally driven mixing in a numerical model of the ocean general circulation. *Ocean Modell.*, **6**, 245–263, doi:10.1016/S1463-5003(03)00011-8.
- Smyth, W. D., J. N. Moum, and D. R. Caldwell, 2001: The efficiency of mixing in turbulent patches: Inferences from direct simulations and microstructure observations. *J. Phys. Oceanogr.*, **31**, 1969–1992, doi:10.1175/1520-0485(2001)031<1969:TEOMIT>2.0.CO;2.
- St. Laurent, L. C., and R. W. Schmitt, 1999: The contribution of salt fingers to vertical mixing in the North Atlantic Tracer Release Experiment. *J. Phys. Oceanogr.*, **29**, 1404–1424, doi:10.1175/1520-0485(1999)029<1404:TCOSFT>2.0.CO;2.
- , and A. M. Thurnherr, 2007: Intense mixing of lower thermocline water on the crest of the Mid-Atlantic Ridge. *Nature*, **448**, 680–683, doi:10.1038/nature06043.
- , J. R. Toole, and R. W. Schmitt, 2001: Buoyancy forcing by turbulence above rough topography in the abyssal Brazil basin. *J. Phys. Oceanogr.*, **31**, 3476–3495, doi:10.1175/1520-0485(2001)031<3476:BFBTAR>2.0.CO;2.
- , H. L. Simmons, and S. R. Jayne, 2002: Estimating tidally driven mixing in the deep ocean. *Geophys. Res. Lett.*, **29**, 21–24, doi:10.1029/2002GL015633.
- Stigebrandt, A., 1976: Vertical diffusion driven by internal waves in a sill fjord. *J. Phys. Oceanogr.*, **6**, 486–495, doi:10.1175/1520-0485(1976)006<0486:VDDBIW>2.0.CO;2.
- , and J. Aure, 1989: Vertical mixing in basin waters of fjords. *J. Phys. Oceanogr.*, **19**, 917–926, doi:10.1175/1520-0485(1989)019<0917:VMIBWO>2.0.CO;2.
- Talley, L. D., 2008: Freshwater transport estimates and the global overturning circulation: Shallow, deep and through-flow components. *Prog. Oceanogr.*, **78**, 257–303, doi:10.1016/j.pocean.2008.05.001.
- , 2013: Closure of the global overturning circulation through the Indian, Pacific and Southern Oceans: Schematics and transports. *Oceanography*, **26**, 80–97, doi:10.5670/oceanog.2013.07.
- , J. L. Reid, and P. E. Robbins, 2003: Data-based meridional overturning streamfunctions for the global ocean. *J. Climate*, **16**, 3213–3226, doi:10.1175/1520-0442(2003)016<3213:DMOSFT>2.0.CO;2.
- Thurnherr, A. M., 2006: Diapycnal mixing associated with an overflow in a deep submarine canyon. *Deep-Sea Res.*, **53**, 194–206, doi:10.1016/j.dsr2.2005.10.020.
- , and K. G. Speer, 2003: Boundary mixing and topographic blocking on the Mid-Atlantic Ridge in the South Atlantic. *J. Phys. Oceanogr.*, **33**, 848–862, doi:10.1175/1520-0485(2003)33<848:BMATBO>2.0.CO;2.
- , L. C. St. Laurent, K. G. Speer, J. M. Toole, and J. R. Ledwell, 2005: Mixing associated with sills in a canyon on the midocean ridge flank. *J. Phys. Oceanogr.*, **35**, 1370–1381, doi:10.1175/JPO2773.1.
- Toole, J. M., R. W. Schmitt, and K. L. Polzin, 1994: Estimates of diapycnal mixing in the abyssal ocean. *Science*, **264**, 1120–1123, doi:10.1126/science.264.5162.1120.
- Waterhouse, A. F., and Coauthors, 2014: Global patterns of diapycnal mixing from measurements of the turbulent dissipation rate. *J. Phys. Oceanogr.*, **44**, 1854–1872, doi:10.1175/JPO-D-13-0104.1.
- Waterman, S., A. C. Naveira Garabato, and K. L. Polzin, 2013: Internal waves and turbulence in the Antarctic Circumpolar Current. *J. Phys. Oceanogr.*, **43**, 259–282, doi:10.1175/JPO-D-11-0194.1.
- , K. L. Polzin, A. C. Naveira Garabato, K. L. Sheen, and A. Forryan, 2014: Suppression of internal wave breaking in the Antarctic Circumpolar Current near topography. *J. Phys. Oceanogr.*, **44**, 1466–1492, doi:10.1175/JPO-D-12-0154.1.
- Watson, A. J., and J. R. Ledwell, 2000: Oceanographic tracer release experiments using sulphur hexafluoride. *J. Geophys. Res.*, **105**, 14 325–14 337, doi:10.1029/1999JC900272.
- Wunsch, C., and R. Ferrari, 2004: Vertical mixing, energy, and the general circulation of the oceans. *Annu. Rev. Fluid Mech.*, **36**, 281–314, doi:10.1146/annurev.fluid.36.050802.122121.